

# XMM-NEWTON/SDSS: STAR FORMATION EFFICIENCY IN GALAXY CLUSTERS AND CONSTRAINTS ON THE MATTER DENSITY PARAMETER

TATIANA F. LAGANÁ<sup>1,2</sup>, YU-YING ZHANG<sup>2,3</sup>, THOMAS H. REIPRICH<sup>2</sup>, AND PETER SCHNEIDER<sup>2</sup>

*Draft version August 1, 2021*

## ABSTRACT

It is believed that the global baryon content of clusters of galaxies is representative of the matter distribution of the universe, and can, therefore, be used to reliably determine the matter density parameter  $\Omega_m$ . This assumption is challenged by the growing evidence from optical and X-ray observations that the total baryon mass fraction increases towards rich clusters. In this context, we investigate the dependence of stellar, and total baryon mass fractions as a function of mass. To do so, we used a subsample of nineteen clusters extracted from the X-ray flux limited sample HIFLUGCS that have available DR-7 *Sloan Digital Sky Survey* (SDSS) data. From the optical analysis we derived the stellar masses. Using XMM-Newton we derived the gas masses. Then, adopting a scaling relation we estimate the total masses. Adding the gas and the stellar mass fractions we obtain the total baryonic content that we find to increase with cluster mass, reaching 7-year *Wilkinson Microwave Anisotropy Probe* (WMAP-7) prediction for clusters with  $M_{500} = 1.6 \times 10^{15} M_\odot$ . We observe a decrease of the stellar mass fraction (from 4.5% to  $\sim 1.0\%$ ) with increasing total mass where our findings for the stellar mass fraction agree with previous studies. This result suggests a difference in the number of stars formed per unit of halo mass, though with a large scatter for low-mass systems. That is, the efficiency of star formation varies on cluster scale that lower mass systems are likely to have higher star formation efficiencies. It follows immediately that the dependence of the stellar mass fraction on total mass results in an increase of the mass-to-light ratio from lower to higher mass systems. We also discuss the consequences of these results in the context of determining the cosmic matter density parameter  $\Omega_m$ .

*Subject headings:* cosmology: observations

## 1. INTRODUCTION

One of the key goals of observational cosmology is to determine the matter density of the universe ( $\Omega_m$ ). One of the classic methods of inferring  $\Omega_m$  is to use the Oort (1958) technique adopting the mass-to-light ratios of galaxy clusters. Independently, one can assume that the ratio of baryonic-to-total mass of very massive galaxy clusters should closely match the ratio of the cosmological parameters, and thus  $\Omega_b/\Omega_m \sim M_b/M_{\text{tot}}$  (White et al. 1993; Evrard 1997; Ettori et al. 2003; Allen et al. 2008).

In these two cases, it is widely believed that the global baryon content and the mass-to-light ratio of galaxy clusters are fairly representative of the matter distribution of the universe, and can therefore be used, to reliably determine the cosmic matter density parameter. Contrary to expectations, this fundamental assumption is challenged by the growing evidence from optical and X-ray observations that the total baryon mass fraction (David et al. 1990; Lin et al. 2003; Gonzalez et al. 2007a; Giodini et al. 2009) and the mass-to-light ratio (e.g., Adami et al. 1998; Girardi et al. 2000; Bahcall & Comerford 2002; Rines et al. 2004; Muzzin et al. 2007) increase towards rich clusters for a broad mass range of systems. Also the comparison between recent direct measurements of the baryon mass content of galaxy clusters and the prediction from the WMAP-7 (Jarosik et al. 2011) presents controversial mass dependence of missing baryons (Andreon

2010; Giodini et al. 2009; Gonzalez et al. 2007b).

Observational difficulties prevented recent studies from building a large sample of galaxy clusters where both masses and luminosities are homogeneously computed, what consequently affect the reliability of  $\Omega_m$  estimates (Girardi et al. 2000). From the optical point of view, the determination of cluster galaxy luminosities is limited by uncertainties related to corrections for Galactic extinction and background galaxy contamination, extrapolation of the luminosity function towards the faint-end, and the completeness of the sample. Also, various methods can be applied to estimate cluster mass. The total masses can be inferred from either X-ray or optical data, under the assumption of hydrostatic equilibrium. Estimates based on gravitational lensing do not require assumptions about the dynamical state of the cluster, but it encompasses substructures along the line of sight. Recent numerical simulations (Meneghetti et al. 2010) claim that combining weak and strong lensing data, the projected masses within  $r_{200}$ <sup>1</sup> can be constrained with a precision of  $\sim 10\%$ . However, deprojection of lensing masses increases the scatter around the true masses by more than a factor of two because of cluster triaxiality. X-ray mass measurements have much smaller scatter (about a factor of two less than the lensing masses), but they are generally biased toward low values between 5% and 10%.

The baryons in galaxy clusters consist of stars in cluster galaxies, intra-cluster light (ICL, stars that are not bounded to the cluster galaxies; e.g., Gonzalez et al. 2007a; Krick & Bernstein 2007), and the hot intra-cluster gas (ICG, Sarazin & Bahcall 1977). The baryonic mass of a galaxy cluster is dominated by the ICG, the mass of which exceeds

<sup>1</sup> Universidade de São Paulo, Instituto de Astronomia, Geofísica e Ciências Atmosféricas, Departamento de Astronomia, Rua do Matão 1226, Cidade Universitária, CEP:05508-090, São Paulo, SP, Brasil.

<sup>2</sup> Argelander-Institut für Astronomie, Universität Bonn, Auf dem Hülgel 71, 53121 Bonn, Germany

<sup>3</sup> National Astronomical Observatories, Chinese Academy of Sciences, Beijing, 100012, China

<sup>1</sup> the radius at which the mean mass density is 200 times the critical density at the cluster redshift.

the mass of the former two components by a factor of  $\sim 6$ . Thus, to reliably compute this cosmological parameter from the baryonic-to-total mass ratio one should address all baryonic components and not only the gas mass. In the past years, measuring individual baryon budget in galaxy clusters became possible with various high-quality optical imaging data (e.g., David et al. 1990; Lin et al. 2003; Roussel et al. 2000; Gonzalez et al. 2007b; Laganá et al. 2008). The combination of the X-ray measured gas mass fraction ( $f_{\text{gas}} = M_{\text{gas}}/M_{\text{tot}}$ , ratio of the gas-to-total mass) with the optically measured stellar mass fraction ( $f_{\star} = M_{\star}/M_{\text{tot}}$ , ratio of the stellar-to-total mass) can thus better constrain the total baryon mass fraction ( $f_b = f_{\star} + f_{\text{gas}}$ ). Notably, these observational measurements are essential to improve our understanding on the distributions of each of these components on cluster scales. Besides, studies of structure formation require constraints on the baryonic components in galaxy clusters to understand star formation and metal enrichment processes.

In this context, HIFLUGCS (Reiprich & Böhringer 2002; Hudson et al. 2010) provides an X-ray flux-limited sample of 64 nearby ( $z \leq 0.1$ ) clusters selected from the *ROSAT* All-Sky Survey (RASS). Nineteen clusters in the HIFLUGCS sample have available *Seventh Data Release of Sloan Digital Sky Survey* data (Abazajian et al. 2009, DR-7 SDSS;). It should be mentioned that the flux-limited samples might be biased towards more luminous clusters, leading to a larger fraction of cool-core clusters for lower mass systems and also they are not necessarily unbiased with respect to morphology (Reiprich 2006). But the advantage of working with flux-limited samples is that the bias can be determined (e.g., Ikebe et al. 2002; Stanek et al. 2006; Eckert et al. 2011).

The investigation of the total baryon mass fraction and mass-to-light ratio dependence on total cluster mass is one of the key goals to understand better the dynamical history of galaxy clusters and also the use of these systems to determine the cosmological parameter  $\Omega_m$ . Thus, in this paper, we analyze the X-ray XMM-*Newton* and optical DR-7 SDSS imaging data for the nineteen above mentioned clusters. It is important to stress that both luminosities and total masses are determined in a homogeneous way. Using the X-ray gas mass as a proxy to determine the total mass seems to be the more suitable technique since it is known that gas mass may likely be unbiased mass proxy (Okabe et al. 2010).

The paper is organized as follows. In Sect. 2 we describe the sample selection criteria providing X-ray and optical details separately. We discuss our results in Sect. 3, and summarize our findings in Sect. 4. The scaling relation used to determine the total mass from the gas mass is given in Appendix A, extra information about the clusters (such as the color-magnitude diagrams, CMD, and luminosity function fits) is given in Appendix B, and a detailed discussion about the main systematic uncertainties involved to derive the stellar masses are presented in Appendix C. Throughout this paper we assume  $\Omega_m = 0.3$ ,  $\Omega_{\Lambda} = 0.7$  and  $H_0 = 70 \text{ km s}^{-1} \text{ Mpc}^{-1}$ . Confidence intervals correspond to the 68% confidence level. We adopted these values to be consistent with the X-ray analysis presented in Zhang et al. (2011a). Even so, it should be noted that the the WMAP-7 parameters for the standard  $\Lambda$ CDM model are  $\Omega_m = 0.267 \pm 0.0288$ ,  $\Omega_{\Lambda} = 0.734 \pm 0.029$ , and  $H_0 = (71 \pm 2.5) \text{ km s}^{-1} \text{ Mpc}^{-1}$ .

## 2. SAMPLE AND DATA ANALYSIS

To constrain the mass dependence of the star formation efficiency (SFE) and baryon mass fraction, it is im-

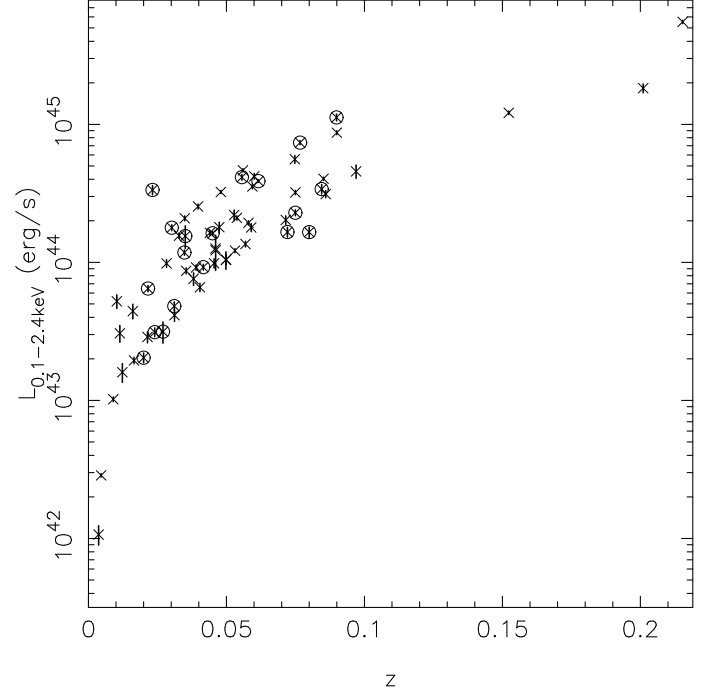


FIG. 1.— XMM-*Newton* measured X-ray bolometric luminosity within the cluster radius  $r_{500}$  in Zhang et al. (2011a) vs. redshift for the HIFLUGCS sample. The 19 clusters with SDSS imaging data are highlighted by circles.

portant to use representative samples. The HIFLUGCS (Reiprich & Böhringer 2002) provides an X-ray flux-limited sample of 64 nearby ( $z \leq 0.1$ ) clusters selected from the RASS. Nineteen clusters in the HIFLUGCS have been observed in the DR-7 SDSS (Abazajian et al. 2009) and are unbiased with respect to the original HIFLUGCS sample, having the same nature of flux selection, as can be seen in Fig. 1.

### 2.1. X-ray data

Detailed XMM-*Newton* data reduction can be found in Zhang et al. (2009, 2011a) including data screening, pointing source subtraction, background modeling, and spectral imaging analysis.

For sample studies, one has to derive all quantities consistently within a characteristic cluster radius. We define them in terms of  $r_{500}$ , the radius at which the mean mass density within the cluster is 500 times the critical density at the cluster redshift.

We can measure  $r_{500}$  from the X-ray measured mass distribution derived under the assumption of hydrostatic equilibrium (HE; e.g. Zhang et al. 2009). However, the present sample contains relaxed and non relaxed clusters where the HE may not be valid (e.g., Zhang et al. 2008, 2010). Thus, we used a scaling relation between the gas and the total mass. To do so, we used 41 dynamically relaxed groups and clusters collected from Vikhlinin et al. (2006a), Arnaud et al. (2007), Böhringer et al. (2007), and Sun et al. (2009). We then fit a power-law to the data points and we used this fit to compute total masses (see Appendix A for more details):

$$\log \left( \frac{M_{500} E(z)}{10^{14} M_{\odot}} \right) = (0.891 \pm 0.017) + \log \left( \frac{M_{\text{gas}} E(z)}{10^{14} M_{\odot}} \right) \times (0.827 \pm 0.022), \quad (1)$$

where  $E(z) = [\Omega_m(1+z)^3 + (1 - \Omega_m - \Omega_\Lambda)(1+z)^2 + \Omega_\Lambda]^{1/2}$ , describing the redshift evolution of the Hubble parameter.

We note that the following scaling relation is based on four different samples of groups and clusters what should reduce the potential bias produced by sample selection. Besides, these 41 systems used to construct our scaling relation are all relaxed systems, and thus the assumption of hydrostatic equilibrium should be valid for these objects and thus minimize the bias in total mass estimates for the clusters in our sample. In the way the total mass is computed,  $\log M_{\text{tot}} = A + B \times \log M_{\text{gas}}$ , when the slope parameter ( $B$  in this case) is positive and lower than 1, the gas mass fraction increases with total mass (see Appendix A for more details).

## 2.2. SDSS data

We selected all HIFLUGCS clusters with DR-7 SDSS (Abazajian et al. 2009) data available. The DR-7 includes more accurate results than previous data releases, updated and more accurate magnitudes for all sources in the *PHOTO* catalog, and better accounting for sky background subtraction. Specifically, we use the *dered* table of magnitudes. Three clusters (A119, NGC507 and, A2063) are located on the border of SDSS field of view, so that we had to exclude them. We ended up with 19 clusters spanning the redshift range of  $0.02 < z < 0.1$  listed in Table 1.

We note that there are 2MASS (Skrutskie et al. 2006) observations for the HIFLUGCS clusters in which the K-band luminosity data have also been used to derive stellar masses. However, SDSS data allow us to make a cleaner selection of the cluster galaxies and to avoid fore- and background contaminations, which are important to derive reliable luminosity functions (LF) and thus the stellar mass for our purpose.

In order to obtain the stellar mass of galaxies we first constructed color-magnitude diagrams (CMD;  $(g-i) \times i$ ) to statistically select cluster members within  $r_{500}$ . In this paper, we fit iteratively the red-sequence (RS), first identified in the  $0.7 < (g-i) < 1.6$  color interval and  $i < 18$  magnitude limit. This interval was the one that best suited the majority of clusters in our sample. For four clusters (IIIZw54, A1367, MKW4, and A400) we had to extend the magnitude limit up to  $i < 16$  to better define the slope of the RS. In this way, we select just the brighter and redder galaxies, what enables us to first identify the red-sequence on the CMD, fitting a linear relation to these galaxies. Then, to constrain the position and the slope of the RS on the CMD, we use the whole color and magnitude interval to re-do the linear fit until it converges. For red galaxies, we adopted  $\pm 0.3$  mag width from the red-sequence best fit. Then, the blue galaxies were considered as the galaxies that lay below the lower limit of the red-sequence (see Figure B.1 in Appendix B). To take into account fore/background contamination we computed the number of galaxies per 0.5 bin of magnitude in an annular region beyond  $8 \times r_{500}$  from the cluster center. We then fit the galaxy number counts in the  $20 < i < 16$  range of magnitude using a power-law. The final cluster magnitude number counts were obtained by subtracting the background fit from the galaxy counts.

For the selected blue and red members, we computed the luminosity function in the  $i$ -band (see Fig. B.1 in Appendix B), performing an analytical fit using two Schechter functions (Schechter 1976) with the usual parameters  $\alpha$  (faint-end slope),  $\Phi^*$  (normalization) and  $M^*$  (characteristic magnitude). For all clusters in our sample but ZwCl1215, A1650, and A2255 we used two Schechter functions to take into account both bright- and faint-end contribution. With the im-

provement of optical instruments, in the past years much work has been done to constrain the faint-population ( $-18 < M_i < -12$ ) of nearby galaxy clusters (e.g., Penny & Conselice 2008; Rines & Geller 2008; Boué et al. 2008). Since the LF of our clusters showed a steep population faintward we fit 2 Schechter functions to describe the overall behavior of galaxies. The covariance between the characteristic magnitude and the power-law index is taken into account (see Appendix B for more details about LF fits).

We considered  $K$ -correction ( $K(z)$ ) and evolutionary correction ( $\epsilon(z)$ ) supplied by Poggianti (1997) to correct  $M^*$  values. To derive the total luminosity we integrated the luminosity function assuming a lower luminosity limit. We thus, assumed the corresponding luminosity of  $M_i = -14.0$  for all clusters, in order to integrate the luminosity function down to the same flux limit. To obtain the stellar masses, we adopted different mass-to-light ratio for ellipticals and spirals, taken from Kauffmann et al. (2003) assuming a Salpeter (1955) initial mass function (IMF), as stated in Equation 21 from Laganá et al. (2008). The stellar mass estimate is tied to the choice of IMF. Changing the IMF scales the stellar mass estimate by a fixed factor, e.g., from a Kroupa (2001) IMF to a Salpeter (1955) IMF with a cut-off at  $0.1 M_\odot$  results in a factor of 2 increase in the stellar mass (e.g., Kauffmann et al. 2003). These procedures were also applied in Zhang et al. (2011b).

When there is a systematic offset between the spectroscopic and photometric magnitudes, the stellar mass estimate can be systematically biased (Kauffmann et al. 2003). The calibration in Fritz et al. (2011) shows that the stellar masses computed from fiber-aperture magnitudes using DR-7 SDSS photometric data are lower by  $\sim 0.15$  dex than the values computed from spectroscopic data. Our sample is in similar redshift and mass ranges as their sample. We, therefore, corrected this bias in our stellar mass estimates using best-fit relation between stellar masses computed from the DR-7 SDSS photometric data and from the spectroscopic data (see the right panel in Fig. 4 in Fritz et al. 2011). All values for stellar masses ( $M_\star^{\text{corr}}$ ) and optical luminosities ( $L_{500}^{\text{corr}}$ ) given in Table 2 are already corrected and are derived on the basis of  $r_{500}$ . We also give the  $\alpha$  and  $M^*$  parameters for the Schechter fit in this table. A detailed discussion about the impact of the main systematic effects on  $M_\star^{\text{corr}}$  and  $L_{500}^{\text{corr}}$  are presented in Appendix C.

## 3. RESULTS: FROM STELLAR MASS FRACTION TO THE COSMOLOGICAL MATTER DENSITY PARAMETER

To fit the trend in our results, we apply the BCES regression fitting method taking into account measurement errors in both variables (Akritas & Bershady 1996). Through this paper, we apply the BCES regression fitting taking into account measurement errors in both variables and their covariance (Akritas & Bershady 1996). Confidence intervals correspond to 68% confidence level.

Figure 2 shows the stellar, and total baryon fraction as a function of total mass. We also compared our result to some previous analyses (Lin et al. 2003; Giodini et al. 2009). We discuss these results in detail in Section 3.1.

In Figure 3, we show the total mass-to-optical light ratio as a function of total mass. This result is specifically discussed in Section 3.2. In Section 3.3 we discuss the consequences of determining the matter-density parameter using galaxy clusters.

TABLE 1  
HIFLUGCS CLUSTERS WITH DR-7 SDSS AVAILABLE DATA

Name	R.A.	DEC	redshift	$r_{500}$ (Mpc)	$M_{\text{gas}}(10^{13} M_{\odot})$	$M_{500}(10^{14} M_{\odot})$
A85	10.46	-9.30	0.0556	$1.216 \pm 0.058$	$7.46 \pm 0.34$	$5.68 \pm 0.81$
A400	44.42	6.02	0.0240	$0.712 \pm 0.034$	$1.00 \pm 0.04$	$1.07 \pm 0.15$
IIIZw54	55.32	15.40	0.0311	$0.731 \pm 0.035$	$1.10 \pm 0.21$	$1.18 \pm 0.17$
A1367	176.01	19.95	0.0216	$0.893 \pm 0.043$	$2.24 \pm 0.07$	$2.11 \pm 0.30$
MKW4	181.11	1.90	0.0200	$0.580 \pm 0.028$	$0.47 \pm 0.02$	$0.58 \pm 0.08$
ZwCl1215	184.42	3.66	0.0750	$1.098 \pm 0.052$	$5.40 \pm 0.29$	$4.34 \pm 0.62$
A1650	194.67	-1.76	0.0845	$1.087 \pm 0.052$	$5.36 \pm 0.90$	$4.28 \pm 0.61$
Coma	194.90	27.96	0.0232	$1.278 \pm 0.061$	$8.18 \pm 0.62$	$6.21 \pm 0.89$
A1795	207.22	26.59	0.0616	$1.118 \pm 0.053$	$5.57 \pm 0.14$	$4.46 \pm 0.63$
MKW8	220.18	3.46	0.0270	$0.715 \pm 0.034$	$1.02 \pm 0.14$	$1.10 \pm 0.16$
A2029	227.73	5.74	0.0767	$1.275 \pm 0.061$	$9.17 \pm 0.33$	$6.81 \pm 0.97$
A2052	229.19	7.02	0.0348	$0.875 \pm 0.042$	$2.13 \pm 0.11$	$2.03 \pm 0.29$
MKW3S	230.47	7.71	0.0450	$0.905 \pm 0.043$	$2.44 \pm 0.10$	$2.29 \pm 0.33$
A2065	230.60	27.71	0.0721	$1.008 \pm 0.048$	$4.12 \pm 1.29$	$3.35 \pm 0.48$
A2142	239.58	27.23	0.0899	$1.449 \pm 0.069$	$15.10 \pm 0.88$	$10.26 \pm 1.47$
A2147	240.57	15.97	0.0351	$1.064 \pm 0.050$	$4.35 \pm 0.43$	$3.63 \pm 0.52$
A2199	247.16	39.55	0.0302	$0.957 \pm 0.045$	$2.90 \pm 0.23$	$2.64 \pm 0.38$
A2255	258.12	64.07	0.0800	$1.072 \pm 0.051$	$5.13 \pm 0.20$	$4.08 \pm 0.58$
A2589	350.99	16.78	0.0416	$0.848 \pm 0.040$	$1.93 \pm 0.12$	$1.88 \pm 0.27$

TABLE 2  
PHOTOMETRIC RESULTS

Name	Bright-end		Faint-end		$L_{500}^{\text{corr}}(10^{12} L_{\odot})$	$M_{\star}^{\text{corr}}(10^{12} M_{\odot})$	$f_{\star}$	$f_{\text{b}}$
	$\alpha_1$	$M_1^*$	$\alpha_2$	$M_2^*$				
A85	$-1.42 \pm 0.09$	$-22.65 \pm 0.32$	$-1.78 \pm 0.080$	$-20.05 \pm 0.51$	$2.32 \pm 0.24$	$6.93 \pm 0.71$	$0.0122 \pm 0.0022$	$0.144 \pm 0.020$
A400	$-1.15 \pm 0.06$	$-22.16 \pm 0.19$	$-1.77 \pm 0.002$	$-18.72 \pm 0.31$	$1.61 \pm 0.20$	$4.93 \pm 0.62$	$0.0459 \pm 0.0087$	$0.139 \pm 0.016$
IIIZw54	$-1.19 \pm 0.08$	$-21.82 \pm 0.65$	$-1.71 \pm 0.044$	$-18.66 \pm 0.64$	$1.38 \pm 0.18$	$3.96 \pm 0.52$	$0.0337 \pm 0.0065$	$0.127 \pm 0.023$
A1367	$-1.27 \pm 0.06$	$-22.66 \pm 0.58$	$-1.84 \pm 0.020$	$-18.18 \pm 0.31$	$1.59 \pm 0.27$	$4.75 \pm 0.80$	$0.0225 \pm 0.0050$	$0.129 \pm 0.016$
MKW4	$-1.10 \pm 0.16$	$-22.00 \pm 0.36$	$-1.78 \pm 0.020$	$-18.01 \pm 0.13$	$0.31 \pm 0.03$	$0.93 \pm 0.11$	$0.0162 \pm 0.0030$	$0.097 \pm 0.012$
ZwCl1215	$-1.64 \pm 0.03$	$-23.13 \pm 0.31$	-	-	$2.71 \pm 0.33$	$8.14 \pm 1.00$	$0.0187 \pm 0.0035$	$0.143 \pm 0.019$
A1650	$-1.67 \pm 0.01$	$-23.25 \pm 0.31$	-	-	$2.24 \pm 0.38$	$6.67 \pm 1.12$	$0.0156 \pm 0.0034$	$0.141 \pm 0.028$
Coma	$-1.26 \pm 0.03$	$-21.95 \pm 0.30$	$-1.98 \pm 0.011$	$-18.06 \pm 0.08$	$4.76 \pm 0.54$	$14.00 \pm 1.59$	$0.0226 \pm 0.0041$	$0.154 \pm 0.022$
A1795	$-1.22 \pm 0.01$	$-21.41 \pm 0.13$	$-1.46 \pm 0.008$	$-19.34 \pm 0.41$	$2.27 \pm 0.34$	$6.99 \pm 1.04$	$0.0157 \pm 0.0032$	$0.141 \pm 0.018$
MKW8	$-1.30 \pm 0.11$	$-21.79 \pm 0.58$	$-1.74 \pm 0.009$	$-18.68 \pm 0.70$	$0.61 \pm 0.09$	$1.76 \pm 0.26$	$0.0161 \pm 0.0033$	$0.109 \pm 0.019$
A2029	$-1.17 \pm 0.07$	$-21.69 \pm 0.17$	$-1.66 \pm 0.020$	$-19.84 \pm 0.12$	$3.18 \pm 0.41$	$9.49 \pm 1.22$	$0.0139 \pm 0.0027$	$0.148 \pm 0.020$
A2052	$-1.27 \pm 0.10$	$-22.10 \pm 0.48$	$-1.70 \pm 0.011$	$-18.59 \pm 0.09$	$1.37 \pm 0.14$	$4.16 \pm 0.42$	$0.0205 \pm 0.0036$	$0.125 \pm 0.016$
MKW3S	$-1.36 \pm 0.03$	$-22.14 \pm 0.48$	$-1.57 \pm 0.041$	$-19.12 \pm 0.25$	$3.13 \pm 0.19$	$9.39 \pm 0.80$	$0.0410 \pm 0.0068$	$0.147 \pm 0.017$
A2065	$-1.10 \pm 0.02$	$-22.00 \pm 0.11$	$-1.62 \pm 0.027$	$-20.08 \pm 0.12$	$2.55 \pm 0.27$	$7.49 \pm 0.57$	$0.0224 \pm 0.0036$	$0.145 \pm 0.042$
A2142	$-1.00 \pm 0.02$	$-21.84 \pm 0.86$	$-1.68 \pm 0.024$	$-20.56 \pm 0.11$	$3.51 \pm 0.19$	$11.00 \pm 0.96$	$0.0107 \pm 0.0018$	$0.158 \pm 0.023$
A2147	$-1.42 \pm 0.05$	$-21.93 \pm 0.12$	$-1.76 \pm 0.015$	$-18.93 \pm 0.12$	$2.24 \pm 0.31$	$6.98 \pm 0.85$	$0.0192 \pm 0.0036$	$0.139 \pm 0.021$
A2199	$-1.18 \pm 0.03$	$-21.80 \pm 0.20$	$-1.86 \pm 0.009$	$-18.28 \pm 0.56$	$1.51 \pm 0.27$	$4.72 \pm 0.56$	$0.0179 \pm 0.0033$	$0.128 \pm 0.018$
A2255	$-1.45 \pm 0.03$	$-23.10 \pm 0.18$	-	-	$2.00 \pm 0.26$	$6.18 \pm 0.79$	$0.0151 \pm 0.0029$	$0.141 \pm 0.019$
A2589	$-1.09 \pm 0.02$	$-21.65 \pm 0.20$	$-1.58 \pm 0.010$	$-18.40 \pm 0.86$	$1.36 \pm 0.14$	$4.19 \pm 0.43$	$0.0223 \pm 0.0039$	$0.125 \pm 0.017$

### 3.1. Star formation efficiency

As clusters of galaxies are the largest virialized systems in the Universe, the baryon budget detected in clusters of galaxies should be relatively representative of the baryon mass fraction estimate of the Universe, when considering very massive halos (e.g., Ettori et al. 2003; Allen et al. 2008).

Thus, the total baryon fraction,  $f_{\text{b}}$ , would simply be given by  $M_{\text{b}} = f_{\text{b}} M_{\text{tot}}$ , where  $M_{\text{b}}$  is the sum of  $M_{\text{gas}} + M_{\star}$ , and  $M_{\text{tot}}$  is the hydrostatic mass. Using our sample of 19 clusters, we investigated the dependence of  $f_{\star}$ , and  $f_{\text{b}}$  as a function of cluster mass.

In Figure 2 we observe a decrease of the stellar mass fraction, and an opposite trend, although less sharply for the gas

mass fraction. More massive clusters have gas mass fraction two times higher and stellar mass fraction around four times lower than less massive clusters. We fit the behavior of the stellar and total baryon-mass fractions with mass as power laws. Within  $r_{500}$  the power-law fit for the stellar-mass fraction is  $f_{\star} = 10^{(-1.54 \pm 0.10)} \times [M_{500}/10^{14} M_{\odot}]^{(-0.36 \pm 0.17)}$ , and the total baryon-mass fraction is given by  $f_{\text{b}} = 10^{(-0.930 \pm 0.018)} \times [M_{500}/10^{14} M_{\odot}]^{(0.136 \pm 0.028)}$ . At this point, we call the attention to the fact that the observed increase of the  $f_{\text{b}}$  with total mass can be partially due to the assumption that the gas mass increases with total mass as discussed in Appendix A.

Our study shows a decrease of the stellar mass fraction from 4.5% to approximately 1.0%, and taking into account



the errors involved, one should notice this dependence deviates from a flat distribution within  $\sim 95\%$  confidence. This result suggests that, at least on cluster scales, the number of stars formed per unit of halo mass between low and high-mass clusters are different, that is the star formation efficiency (SFE) depends on the environment (as already addressed in several papers Gonzalez et al. 2000; Lin et al. 2003; Laganá et al. 2008; Ettori et al. 2009; Zhang et al. 2011b). In massive clusters, more hot gas and dark matter is settled in the deep potential wells than the amount of individual galaxies. In low-mass systems, the accretion of individual less massive galaxies is more important and more low entropy gas is brought in to form stars. Both processes result in lower star formation efficiency for more massive systems.

As a consequence of the dependence of the baryon mass fractions on total mass, one does not observe a “flat”  $f_b$  distribution as a function of the total mass on cluster scales. As shown in Figure 2, the total baryon mass fraction is lower than the WMAP-7 predicted cosmic fraction, in line with previous studies, e.g., Ettori (2003); McCarthy et al. (2007), but see Simionescu et al. (2011). In particular, the discrepancy between the observed and the fit value becomes larger with decreasing mass reaching  $\sim 5.5\sigma$  for systems with masses below  $3 \times 10^{14} M_\odot$ , and  $\sim 3\sigma$  for systems with their masses higher  $3 \times 10^{14} M_\odot$ . The disagreement between observations and WMAP result has been already pointed out: Gonzalez et al. (2007b) presented a  $3.2\sigma$  discrepancy, Giodini et al. (2009) found a  $5\sigma$  disparity, and more recently Andreon (2010) showed a  $6\sigma$  distinction. These studies analyzed cluster and groups sample in a similar mass range as the one used in this work ( $5 \times 10^{13} M_\odot - 10^{15} M_\odot$ ). Giodini et al. (2009) analyzed 91 objects spanning a range in  $M_{500}$  of  $\sim 10^{13} - 10^{15} M_\odot$ . Andreon (2010) investigated 52 clusters and groups in the same mass range as the latter authors, and Gonzalez et al. (2007b) considered 24 galaxy clusters in a broader interval of mass, ranging from  $M_{500} = 10^{12} M_\odot$  up to  $M_{500} \sim 8 \times 10^{14} M_\odot$ .

It is worth noting that the most massive cluster in our sample has a total mass of  $M \sim 10^{15} M_\odot$  and its baryon mass fraction already reaches  $\sim 96\%$  of the cosmic value. Extrapolating our fit for the total baryon mass fraction,  $f_b$  reaches the WMAP-7 prediction for clusters with  $M \geq 1.6 \times 10^{15} M_\odot$ . We show the ratio between observed and WMAP-7 values for  $f_b$  as a function of total mass in the lower panel of Fig. 2. Hydrodynamical simulations claim that baryons in clusters have undergone a large depletion during the formation of these structures.

Although White et al. (1993) claim that within a sufficiently large radius the mean baryon fraction must take the global value, Frenk et al. (1999) assert that the depletion parameter, that is the ratio between the observed and the predicted baryon mass fraction is  $\Upsilon = 0.925$ , which is in line with more recent estimate (e.g., Ettori et al. 2006; Young et al. 2011). This means that even considering a large radius, e.g.  $r_{200}$ , some baryons are missing also in massive clusters.

The comparison of the observed baryon budget to the WMAP-7 cosmic fraction (Jarosik et al. 2011) consistently suggests that the amount of missing baryons increases toward low-mass systems. Recently, Dai et al. (2010) proposed that the baryon loss mechanism is primarily controlled by the depth of the potential well of the system. For deep potential wells, such as rich clusters, baryon loss is not significant, however, for lower-mass clusters, baryon loss becomes increasingly important. Such a mechanism could be the pre-

heating of baryons before they collapse. In this picture, the baryons never fall into groups and low-mass clusters, but remain well beyond  $r_{200}$ . Alternatively, the gas falls into the potential-wells and is subsequently removed by feedback provided from SNe and AGNs, which should also play a major role for low-mass systems.

Some missing baryons are suggested, which can partially account for the discrepancy between the observed and the predicted cosmic baryon mass fraction. Intra-cluster light (ICL) is one of the most important missing baryons. Observational results have shown that the ICL can account for 6%–22% of the total cluster light in the  $r$ -band (e.g., Krick & Bernstein 2007; Gonzalez et al. 2007b; Pierini et al. 2008), and being an order of magnitude lower, it would account for  $\sim 2\%$  in the total baryon mass fraction. Recent numerical simulations performed by Puchwein et al. (2010) showed that the amount of gas and ICL removed by active galactic nucleus (AGN) heating from the central regions of clusters and driven outwards ( $r > r_{500}$ ) depends on cluster mass, being higher in low-mass systems. Puchwein et al. (2010) estimate that for a cluster with total mass  $M = 4 \times 10^{13} M_\odot$  the ICL account for 58% of the total stars. Considering this latter result, there is no significant missing baryons as suggested by e.g. Afshordi et al. (2007). Just the ICL and some part of the ICG would be sufficient to explain the difference between observations and cosmological prediction. However, such high amount of ICL would be visible in current observations.

Another reasonable possibility is a dependence of the baryon budget as a function of radius (e.g., Henriksen & Mamon 1994; Ettori & Fabian 1999). It might be that in the limiting radius of X-ray observations ( $r_{500}$ ) the total baryon budget is still underestimated. Although Allen et al. (2002) show that the gas mass fractions in the clusters asymptote towards an approximately constant value at a radius  $r_{2500}$ , most of the numerical simulation results and observational data show an evident increase of the baryonic content with cluster radius. Vikhlinin et al. (2006b) showed that the gas mass fraction increases with radius as a power law of overdensity. Recently, Simionescu et al. (2011) showed that the baryon mass fraction increases dramatically with cluster radius for the Perseus cluster. This cluster is one of the few clusters having deepest X-ray data to measure the baryon mass fraction up to the virial radii. They found that, for the Perseus cluster, the gas mass fraction alone (without considering the stars) reaches the baryonic cosmic mean value at about half of  $r_{200}$  and at  $r_{200}$  it is  $\sim 38\%$  above the mean baryonic value. However, it is important to have in mind that this is an isolate result and it is important to analyze the dependence of  $f_{\text{gas}}$  (determined within the virial radius) on total mass for a sample of clusters. For instance, Reiprich (2003) studied the gas mass fraction within  $r_{200}$  for 106 clusters, and Perseus is among the five clusters with the highest  $f_{\text{gas}}$ . This study can be readdressed using Suzaku data.

### 3.2. Total mass-to-optical light ratio

In this work we used independent X-ray and optical methods to compute the total mass-to-optical light ratio for our sample, and both optical luminosities and total masses were homogeneously determined. Compared to other estimates, the determination of total masses using X-ray is a robust and a preferable method since it involves lower uncertainties (Nagai et al. 2007; Meneghetti et al. 2010).

For  $\Lambda$ CDM cosmological model, the mass-to-light ratio

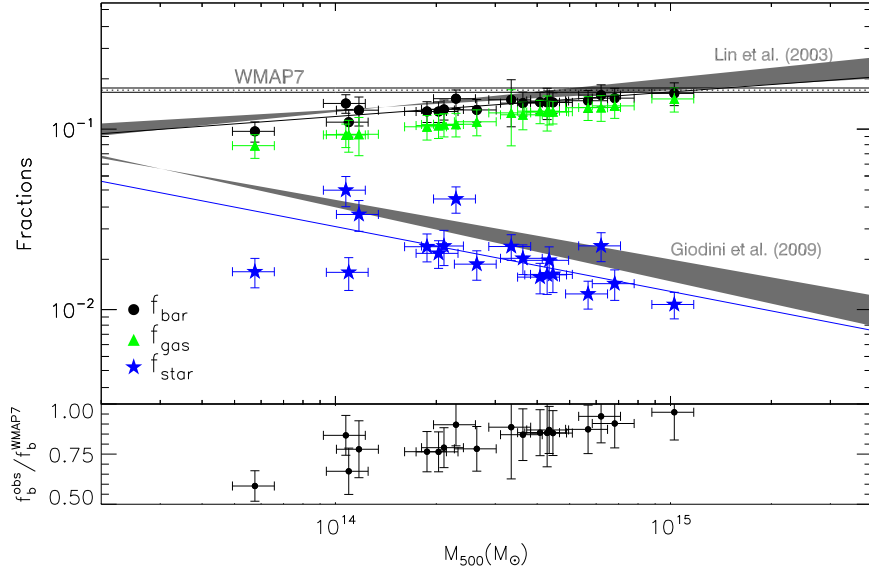


FIG. 2.— *Upper panel*: Total baryon-mass fraction (black circles), gas-mass fraction (green triangles) and stellar-mass fraction (blue stars) as functions of the total mass. The black and the blue solid lines represent power-law fits for the total baryon and stellar mass fractions as a function of total mass, respectively. The horizontal lines on the top of the plot represent the WMAP-7 result ( $f_{\text{bar}}^{\text{WMAP-7}} = 0.171 \pm 0.009$  Jarosik et al. 2011) with 1 sigma error. For comparison, we also show the best-fit for the baryon-mass fraction from Lin et al. (2003) and for the stellar mass fraction from Giodini et al. (2009). *Lower panel*: Ratio between observational and WMAP-7 baryon mass fraction as a function of total mass.

( $M/L$ ) in high-mass systems is supposed to be approximately independent of halo mass. It has been generally found that  $M/L$  increases with halo mass but there is an approximate plateau in  $M/L$  values for the richest bound systems (e.g., David et al. 1995; Cirimele et al. 1997; Sheldon et al. 2009). The existence of this plateau is sometimes taken as evidence that the measured values of  $M/L$  do indeed represent the universal value.

However, recently, most authors have found a dependence between the  $M/L$  and the total mass, even for massive clusters of galaxies. Assuming a power-law relation,  $M_{500}/L_\star \propto M_{500}^\alpha$ , those authors have found  $\alpha$  to be in the range of 0.2–0.4, in both optical and near-infrared bands, over a large mass range (Adami et al. 1998; Bahcall & Comerford 2002; Rines et al. 2004).

In Figure 3 we show the dependence of the total mass-to-optical light ratio ( $M_{500}/L_\star$ ) on total mass. The best-fit for the mass-to-optical light ratio follows  $M_{500}/L_\star = 10^{(2.02 \pm 0.10)} \times [M_{500}/10^{14} M_\odot]^{(0.361 \pm 0.169)}$ . Considering the sample analysed in this work, a plateau is not clearly present for the massive end, and the best-fit leads to a  $M_{500}/L_\star = 241 M_\odot/L_\odot$  for clusters with total mass of  $10^{15} M_\odot$ .

We see from Figure 3 that non cool-core clusters present a higher dispersion when compared to cool-core clusters. This may indicate that the dynamical state of the cluster should be considered when analyzing the mass-to-light ratio, because it might follow that for a large and homogeneous sample of cool-core clusters a plateau becomes more evident. Thus, in order to better investigate whether there is a plateau at the massive end, further studies should consider a complete flux-limited sample of cool-core clusters.

The dependence of  $M_{500}/L_\star$  shown in Figure 3 with cluster mass is a direct consequence of the varying star formation efficiency in galaxy clusters. Since low-mass systems have

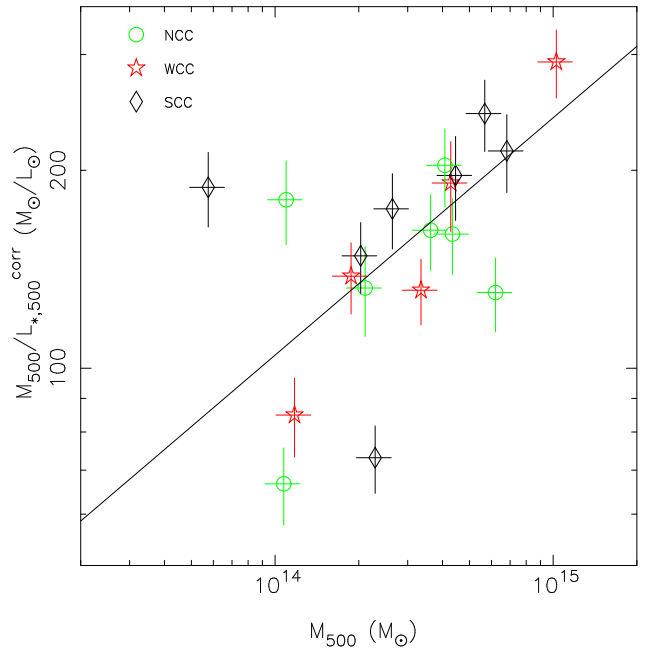


FIG. 3.— Total mass-to-light ratio as a function of total mass of the system. The black, red and green colors denote strong, weak cool-core and non cool-core clusters, respectively.

higher star formation efficiency compared to a massive cluster, the optical light will not vary uniformly and thus, the total mass-to-optical light shows a dependence on cluster mass.

### 3.3. The cosmological parameter $\Omega_m$

The results presented in the Sections 3.1 and 3.2 have important implications on the cosmological use of galaxy clusters. Using the Oort (1958) technique, one can determine the

matter density parameter following  $\Omega_m = (M/L) \times \rho_L/\rho_c$ , where  $\rho_c$  is the critical density, and  $\rho_L$  is the typical luminosity density of the universe. A fundamental assumption in this application is that  $M/L$  of clusters is a fairly representative measurement of the universal value. However, the mass-to-light ratio has been found to increase with cluster mass. Assuming the mass-to-light ratio range shown in Figure 3 (from  $70 M_\odot/L_\odot$  up to  $300 M_\odot/L_\odot$ ), and adopting  $j_i \sim 2.12 \times 10^8 h_{100} L_\odot/\text{Mpc}^3$  for the luminosity density (see Table 3 from Blanton et al. 2003), we have the total matter density parameter spanning the range  $0.07 < \Omega_m < 0.27$ . Taking into account the errors involved in this method to derive both total mass ( $\sim 10\%$ ) and the optical light (a mean value of about  $20\%$ ), we can determine  $\Omega_m$  within  $\sim 14\%$  of uncertainty. It should be noted that since we did not reach the claimed plateau in mass-to-light ratio towards the massive end, the upper limit obtained here for the matter density parameter ( $\Omega_m = 0.3$ ), although consistent with the WMAP-7 concordance value within the errors (Jarosik et al. 2011), could still be an underestimate of  $\Omega_m$ .

Another way to determine the matter density parameter is considering that the ratio of baryonic-to-total mass in clusters should closely match the cosmological parameters  $\Omega_b/\Omega_m$ . Thus, adopting  $\Omega_b h^2 = 0.02260 \pm 0.00053$  (Jarosik et al. 2011), and the total baryon fraction computed in this work (and listed in Table 2) we obtained  $0.15 < \Omega_m < 0.30$ , a narrower interval compared to the previous method. This shows that the stellar and gas mass estimates from optical and X-ray data provide better determination of  $\Omega_m$  when compared to the use of  $M_{500}/L_\star$ . The first advantage is that to derive the gas mass one does not assume hydrostatic equilibrium, and thus the dynamical state of the cluster will not bias this determination. Then, the uncertainties involved in this determination are around  $5\%$ - $10\%$  (Nagai et al. 2007; Meneghetti et al. 2010). Also, X-ray gives a 3D view of the cluster when deprojection is done, while total light is always derived from a 2D projection of galaxies in the CMD. There are also the difficulties already pointed out in the Section 1 and discussed in Girardi et al. (2000) related to the luminosity estimates. Moreover, there has been some concern with the  $M/L$  method because recent numerical simulations suggest that light is a biased tracer of dark matter, providing a biased value for  $\Omega_m$  (Ostriker et al. 2003). The Oort method Oort (1958) necessarily focus on denser regions of the galaxy distribution, and thus the estimate of  $\Omega_m$  relies on the assumption that the galaxy population in these regions is representative of the universe as a whole. However, it is well-known that the galaxy population in clusters differs from the field population since the work from Dressler (1980). Since rich clusters of galaxies encompasses large regions (of several Mpc), observations that extend up to the virial radius ( $r \sim r_{200}$ ) should, in principle, contain a sufficient collapsed region and provide a fair mass-to-light ratio. Nevertheless, it is important to stress that in this work we just examine a cluster volume of radius  $r_{500}$ , what can also affect our estimates.

It is worth mentioning the effect of the ICL on both determinations. In both cases, the ICL would contribute to lower the  $\Omega_m$  estimates. Using the Oort (1958) technique, the ICL would account for the total light and then this ratio would be smaller than the ones obtained here. Thus, if on the one hand the upper limit for  $\Omega_m$  could still be higher when reaching the plateau for massive clusters; on the other hand, the inclusion of the ICL can contribute to a lower estimate of the matter density parameter. Furthermore, using the total

baryon-to-mass fraction, the matter density parameter is given by  $\Omega_m \sim \Omega_b \times M_{\text{tot}}/M_b$ , and the ICL would account for the total baryon estimates ( $M_b$ ). Consequently one would obtain a lower determination of the matter density parameter. Thus, in both cases, the derived values in this work are biased up for not considering the ICL contribution.

#### 4. CONCLUSIONS

We studied a representative sample of 19 clusters, and investigated this sample as a robust local reference to constrain the baryon mass fraction and its mass dependence on cluster scales for future studies. Our conclusions are as follows.

- We obtained optical luminosities and total masses for a sample of 19 clusters in a homogeneous way. Thus, we computed total mass-to-optical light ratio using two independent methods, what present a considerable advantage over previous studies.
- The total mass-to-optical light ratio decreases toward low-mass systems, following the relation  $M_{500}/L_\star = 10^{(2.02 \pm 0.10)} \times [M_{500}/10^{14} M_\odot]^{(0.361 \pm 0.169)}$ . This result is a direct consequence of the varying SFE in cluster scales. In this work the  $M_{500}/L_\star$  varies from  $\sim 60 M_\odot/L_\odot$  up to almost  $300 M_\odot/L_\odot$ . Total mass-to-optical light ratio does not show evidence of a flattening, and the best-fit leads to a  $M_{500}/L_\star = 241 M_\odot/L_\odot$  for clusters with total mass of  $10^{15} M_\odot$ . Our results indicate that this flattening towards massive clusters should be more evident when considering a flux-limited sample of cool-core clusters. We observed that non cool-core clusters present a large dispersion when compared to more relaxed systems and may introduce some bias in the final dependence.
- Both  $f_b$  and  $f_\star$  show a mass dependence. Within  $r_{500}$ , the power-law fits are  $f_\star = 10^{(-1.54 \pm 0.10)} \times [M_{500}/10^{14} M_\odot]^{(-0.359 \pm 0.170)}$ , and  $f_b = 10^{(-0.93 \pm 0.018)} \times [M_{500}/10^{14} M_\odot]^{(0.136 \pm 0.028)}$  for the stellar, and total baryon mass fraction, respectively. The observed increase of the  $f_b$  with total mass can be partially due to the increase of the gas mass with total mass as discussed in Appendix A. Toward the high-mass end, the value gradually approaches the WMAP-7 prediction, reaching it at  $M_{500} = 1.6 \times 10^{15} M_\odot$ , when extrapolating our fit for the total baryon mass fraction. However, the most massive cluster in our sample has a total mass of  $M_{500} = 1.026 \times 10^{15} M_\odot$  and its baryon mass fraction already reaches  $\sim 96\%$  of the cosmic value. The amount of missing baryons with respect to the WMAP-7 predicted fraction increases toward lower systems. This can be compensated by ICL and a significant part of the gas that is driven outwards ( $r > r_{500}$ ) due to AGN feedback, especially in lower mass-systems.
- The SFE is lower in more massive clusters, increasing towards the low-mass end. The rapid decrease observed in the stellar mass fraction as a function of total mass suggests a significant change in the efficiency of star formation with cluster mass (as already addressed in several papers: Gonzalez et al. 2000; Lin et al. 2003; Laganá et al. 2008; Ettori et al. 2009).
- We derived the matter density parameter using the Oort (1958) technique and also from the baryon-to-total



mass ratio. Using these two approaches, we obtained  $0.07 < \Omega_m < 0.3$  and  $0.15 < \Omega_m < 0.27$ , respectively. Using the baryon-to-total mass ratio to compute  $\Omega_m$  seems to give narrower range and more accurate values. Since we did not consider the ICL contribution, the obtained values for the matter-density parameter are possibly biased low.

The XMM-Newton project is an ESA Science Mission with instruments and contributions directly funded by ESA Member States and the USA (NASA). The XMM-Newton project is supported by the Bundesministerium für Wirtschaft und Technologie/Deutsches Zen-

trum für Luft- und Raumfahrt (BMWi/DLR, FKZ 50 OX 0001) and the Max-Planck Society. We thank the referee, Stefano Ettori, for relevant questions and fruitful discussions that improved the quality of this manuscript. T. F. L. acknowledges G. B. Lima Neto and F. Durret for constructive discussions. T. F. L. also thanks the financial support from FAPESP (grants: 2006/56213-9, 2008/04318-7) and CAPES (grant: BEX3405-10-9). We thank Jacopo Fritz for providing the best-fit relation between stellar masses computed from the DR-7 SDSS photometric and spectroscopic data. Y. Y. Z. also acknowledges support from the German BMBF through the Verbundforschung under grant 50 OR 1005. T. H. R. acknowledges support by the DFG through Heisenberg grant 1462/5. This work was supported by the Deutsche Forschungsgemeinschaft under the Collaborative Research Center TR-33.

## REFERENCES

- Abazajian, K. N., Adelman-McCarthy, J. K., Agüeros, M. A., Allam, S. S., Allende Prieto, C., An, D., Anderson, K. S. J., Anderson, S. F., Annis, J., Bahcall, N. A., & Bailer-Jones, C. A. L. 2009, *ApJS*, 182, 543
- Adami, C., Biviano, A., & Mazure, A. 1998, *A&A*, 331, 439
- Afshordi, N., Lin, Y., Nagai, D., & Sanderson, A. J. R. 2007, *MNRAS*, 378, 293
- Akritas, M. G. & Bershady, M. A. 1996, *ApJ*, 470, 706
- Allen, S. W., Rapetti, D. A., Schmidt, R. W., Ebeling, H., Morris, R. G., & Fabian, A. C. 2008, *MNRAS*, 383, 879
- Allen, S. W., Schmidt, R. W., & Fabian, A. C. 2002, *MNRAS*, 334, L11
- Andreon, S. 2010, *MNRAS*, 407, 263
- Arnaud, M., Pointecouteau, E., & Pratt, G. W. 2007, *A&A*, 474, L37
- Bahcall, N. A. & Comerford, J. M. 2002, *ApJ*, 565, L5
- Blanton, M. R., Hogg, D. W., Bahcall, N. A., Brinkmann, J., Britton, M., Connolly, A. J., Csabai, I., Fukugita, M., Loveday, J., Meiksin, A., Munn, J. A., Nichol, R. C., Okamura, S., Quinn, T., Schneider, D. P., Shimasaku, K., Strauss, M. A., Tegmark, M., Vogeley, M. S., & Weinberg, D. H. 2003, *ApJ*, 592, 819
- Böhringer, H., Schuecker, P., Pratt, G. W., Arnaud, M., Ponman, T. J., Croston, J. H., Borgani, S., Bower, R. G., Briel, U. G., Collins, C. A., Donahue, M., Forman, W. R., Finoguenov, A., Geller, M. J., Guzzo, L., Henry, J. P., Kneissl, R., Mohr, J. J., Matsushita, K., Mullis, C. R., Ohashi, T., Pedersen, K., Pierini, D., Quintana, H., Raychaudhury, S., Reiprich, T. H., Romer, A. K., Rosati, P., Sabirli, K., Temple, R. F., Viana, P. T. P., Vikhlinin, A., Voit, G. M., & Zhang, Y. 2007, *A&A*, 469, 363
- Boué, G., Adami, C., Durret, F., Mamon, G. A., & Cayatte, V. 2008, *A&A*, 479, 335
- Bower, R. G., Lucey, J. R., & Ellis, R. S. 1992a, *MNRAS*, 254, 601
- . 1992b, *MNRAS*, 254, 589
- Crimele, G., Nesci, R., & Trevese, D. 1997, *ApJ*, 475, 11
- Dai, X., Bregman, J. N., Kochanek, C. S., & Rasia, E. 2010, *ApJ*, 719, 119
- David, L. P., Arnaud, K. A., Forman, W., & Jones, C. 1990, *ApJ*, 356, 32
- David, L. P., Jones, C., & Forman, W. 1995, *ApJ*, 445, 578
- De Propriis, R., Colless, M., Driver, S. P., Couch, W., Peacock, J. A., Baldry, I. K., Baugh, C. M., Bland-Hawthorn, J., Bridges, T., Cannon, R., Cole, S., Collins, C., Cross, N., Dalton, G. B., Efsthathiou, G., Ellis, R. S., Frenk, C. S., Glazebrook, K., Hawkins, E., Jackson, C., Lahav, O., Lewis, I., Lumsden, S., Maddox, S., Madgwick, D. S., Norberg, P., Percival, W., Peterson, B., Sutherland, W., & Taylor, K. 2003, *MNRAS*, 342, 725
- Dressler, A. 1980, *ApJ*, 236, 351
- Eckert, D., Molendi, S., & Paltani, S. 2011, *A&A*, 526, A79+
- Ettori, S. 2003, *MNRAS*, 344, L13
- Ettori, S., Dolag, K., Borgani, S., & Murante, G. 2006, *MNRAS*, 365, 1021
- Ettori, S. & Fabian, A. C. 1999, *MNRAS*, 305, 834
- Ettori, S., Morandi, A., Tozzi, P., Balestra, I., Borgani, S., Rosati, P., Lovisari, L., & Terenziani, F. 2009, *A&A*, 501, 61
- Ettori, S., Tozzi, P., & Rosati, P. 2003, *A&A*, 398, 879
- Evrard, A. E. 1997, *MNRAS*, 292, 289
- Frenk, C. S., White, S. D. M., Bode, P., Bond, J. R., Bryan, G. L., Cen, R., Couchman, H. M. P., Evrard, A. E., Gnedin, N., Jenkins, A., Khokhlov, A. M., Klypin, A., Navarro, J. F., Norman, M. L., Ostriker, J. P., Owen, J. M., Pearce, F. R., Pen, U., Steinmetz, M., Thomas, P. A., Villumsen, J. V., Wadsley, J. W., Warren, M. S., Xu, G., & Yepes, G. 1999, *ApJ*, 525, 554
- Fritz, J., Poggianti, B. M., Cava, A., Valentinuzzi, T., Moretti, A., Bettoni, D., Bressan, A., Couch, W. J., D'Onofrio, M., Dressler, A., Fasano, G., Kjærgaard, P., Moles, M., Omizzolo, A., & Varela, J. 2011, *A&A*, 526, A45
- Giodini, S., Pierini, D., Finoguenov, A., Pratt, G. W., Böhringer, H., Leauthaud, A., Guzzo, L., Aussel, H., Bolzonella, M., Capak, P., Elvis, M., Hasinger, G., Ilbert, O., Kartaltepe, J. S., Koekemoer, A. M., Lilly, S. J., Massey, R., McCracken, H. J., Rhodes, J., Salvato, M., Sanders, D. B., Scoville, N. Z., Sasaki, S., Smolcic, V., Taniguchi, Y., Thompson, D., & the COSMOS Collaboration. 2009, *ApJ*, 703, 982
- Girardi, M., Borgani, S., Giuricin, G., Mardirossian, F., & Mezzetti, M. 2000, *ApJ*, 530, 62
- Gladders, M. D., Lopez-Cruz, O., Yee, H. K. C., & Kodama, T. 1998, *ApJ*, 501, 571
- Gonzalez, A. H., Zabludoff, A. I., Zaritsky, D., & Dalcanton, J. J. 2000, *ApJ*, 536, 561
- Gonzalez, A. H., Zaritsky, D., & Zabludoff, A. I. 2007a, *ApJ*, 666, 147
- . 2007b, *ApJ*, 666, 147
- Henriksen, M. J. & Mamon, G. A. 1994, *ApJ*, 421, L63
- Hudson, D. S., Mittal, R., Reiprich, T. H., Nulsen, P. E. J., Andernach, H., & Sarazin, C. L. 2010, *A&A*, 513, A37+
- Ikebe, Y., Reiprich, T. H., Böhringer, H., Tanaka, Y., & Kitayama, T. 2002, *A&A*, 383, 773
- Jarosik, N., Bennett, C. L., Dunkley, J., Gold, B., Greason, M. R., Halpern, M., Hill, R. S., Hinshaw, G., Kogut, A., Komatsu, E., Larson, D., Limon, M., Meyer, S. S., Nolte, M. R., Odgaard, N., Page, L., Smith, K. M., Spergel, D. N., Tucker, G. S., Weiland, J. L., Wollack, E., & Wright, E. L. 2011, *ApJS*, 192, 14
- Kauffmann, G. & Charlot, S. 1998, *MNRAS*, 294, 705
- Kauffmann, G., Heckman, T. M., White, S. D. M., Charlot, S., Tremonti, C., Brinchmann, J., Bruzual, G., Peng, E. W., Seibert, M., Bernardi, M., Blanton, M., Brinkmann, J., Castander, F., Csabai, I., Fukugita, M., Ivezić, Z., Munn, J. A., Nichol, R. C., Padmanabhan, N., Thakar, A. R., Weinberg, D. H., & York, D. 2003, *MNRAS*, 341, 33
- Kodama, T. & Arimoto, N. 1997, *A&A*, 320, 41
- Krick, J. E. & Bernstein, R. A. 2007, *AJ*, 134, 466
- Kroupa, P. 2001, *MNRAS*, 322, 231
- Laganá, T. F., Lima Neto, G. B., Andrade-Santos, F., & Cypriano, E. S. 2008, *A&A*, 485, 633
- Lin, Y., Mohr, J. J., & Stanford, S. A. 2003, *ApJ*, 591, 749
- Maughan, B. J. 2007, *ApJ*, 668, 772
- McCarthy, I. G., Bower, R. G., & Balogh, M. L. 2007, *MNRAS*, 377, 1457
- Meneghetti, M., Rasia, E., Merten, J., Bellagamba, F., Ettori, S., Mazzotta, P., Dolag, K., & Marri, S. 2010, *A&A*, 514, A93+
- Muzzin, A., Yee, H. K. C., Hall, P. B., & Lin, H. 2007, *ApJ*, 663, 150
- Nagai, D., Kravtsov, A. V., & Vikhlinin, A. 2007, *ApJ*, 668, 1
- Okabe, N., Zhang, Y., Finoguenov, A., Takada, M., Smith, G. P., Umetsu, K., & Futamase, T. 2010, *ApJ*, 721, 875
- Oort, J. H. 1958, ed. R. Stoopes (Brussel: Solvey Inst), 163
- Ostriker, J. P., Nagamine, K., Cen, R., & Fukugita, M. 2003, *ApJ*, 597, 1
- Penny, S. J. & Conselice, C. J. 2008, *MNRAS*, 383, 247
- Pierini, D., Zibetti, S., Braglia, F., Böhringer, H., Finoguenov, A., Lynam, P. D., & Zhang, Y. 2008, *A&A*, 483, 727
- Poggianti, B. M. 1997, *A&AS*, 122, 399
- Puchwein, E., Springel, V., Sijacki, D., & Dolag, K. 2010, *MNRAS*, 406, 936
- Reiprich, T. H. 2003, *arXiv:astro-ph/0308137*
- . 2006, *A&A*, 453, L39
- Reiprich, T. H. & Böhringer, H. 2002, *ApJ*, 567, 716
- Rines, K. & Geller, M. J. 2008, *AJ*, 135, 1837
- Rines, K., Geller, M. J., Diaferio, A., Kurtz, M. J., & Jarrett, T. H. 2004, *AJ*, 128, 1078
- Romeo, A. D., Napolitano, N. R., Covone, G., Sommer-Larsen, J., Antonuccio-Delogo, V., & Capaccioli, M. 2008, *MNRAS*, 389, 13
- Roussel, H., Sadat, R., & Blanchard, A. 2000, *A&A*, 361, 429
- Salpeter, E. E. 1955, *ApJ*, 121, 161
- Sarazin, C. L. & Bahcall, J. N. 1977, *ApJS*, 34, 451
- Schechter, P. 1976, *ApJ*, 203, 297
- Sheldon, E. S., Johnston, D. E., Masjedi, M., McKay, T. A., Blanton, M. R., Scranton, R., Wechsler, R. H., Koester, B. P., Hansen, S. M., Frieman, J. A., & Annis, J. 2009, *ApJ*, 703, 2232
- Simionescu, A., Allen, S. W., Mantz, A., Werner, N., Takei, Y., Morris, R. G., Fabian, A. C., Sanders, J. S., Nulsen, P. E. J., George, M. R., & Taylor, G. B. 2011, *Science*, 331, 1576



Skrutskie, M. F., Cutri, R. M., Stiening, R., Weinberg, M. D., Schneider, S., Carpenter, J. M., Beichman, C., Capps, R., Chester, T., Elias, J., Huchra, J., Liebert, J., Lonsdale, C., Monet, D. G., Price, S., Seitzer, P., Jarrett, T., Kirkpatrick, J. D., Gizis, J. E., Howard, E., Evans, T., Fowler, J., Fullmer, L., Hurt, R., Light, R., Kopan, E. L., Marsh, K. A., McCallon, H. L., Tam, R., Van Dyk, S., & Wheelock, S. 2006, *AJ*, 131, 1163  
 Stanek, R., Evrard, A. E., Böhringer, H., Schuecker, P., & Nord, B. 2006, *ApJ*, 648, 956  
 Sun, M., Voit, G. M., Donahue, M., Jones, C., Forman, W., & Vikhlinin, A. 2009, *ApJ*, 693, 1142  
 Vikhlinin, A., Kravtsov, A., Forman, W., Jones, C., Markevitch, M., Murray, S. S., & Van Speybroeck, L. 2006a, *ApJ*, 640, 691  
 —. 2006b, *ApJ*, 640, 691

White, S. D. M., Navarro, J. F., Evrard, A. E., & Frenk, C. S. 1993, *Nature*, 366, 429  
 Young, O. E., Thomas, P. A., Short, C. J., & Pearce, F. 2011, *MNRAS*, 413, 691  
 Zhang, Y., Andernach, H., Caretta, C. A., Reiprich, T. H., Böhringer, H., Puchwein, E., Sijacki, D., & Girardi, M. 2011a, *A&A*, 526, A105+  
 Zhang, Y., Finoguenov, A., Böhringer, H., Kneib, J., Smith, G. P., Kneissl, R., Okabe, N., & Dahle, H. 2008, *A&A*, 482, 451  
 Zhang, Y., Okabe, N., Finoguenov, A., Smith, G. P., Piffaretti, R., Valdarnini, R., Babul, A., Evrard, A. E., Mazzotta, P., Sanderson, A. J. R., & Marrone, D. P. 2010, *ApJ*, 711, 1033  
 Zhang, Y., Reiprich, T. H., Finoguenov, A., Hudson, D. S., & Sarazin, C. L. 2009, *ApJ*, 699, 1178  
 Zhang, Y.-Y., Laganá, T. F., Pierini, D., Puchwein, E., Schneider, P., & Reiprich, T. H. 2011b, *ArXiv:1109.0390*

## APPENDIX

### A. $M_{\text{GAS}}-M_{500}$ RELATION

Since total mass estimates are derived under the assumption of hydrostatic equilibrium (EQ), and the present sample contains clusters in a wide variety of dynamical states (here separated in strong cool-core, weak cool-core and non cool-core clusters), the EQ assumption may not be valid in all cases. Thus, we preferred to derive total masses using the scaling relation. Recent observational investigations using a variety of cluster samples have demonstrated that the gas mass is indeed a low-scatter mass proxy (Maughan 2007; Arnaud et al. 2007). To construct a scaling-relation between total and gas mass, as shown in Fig. 1, we used 41 dynamically relaxed clusters from Vikhlinin et al. (2006a), Arnaud et al. (2007), Böhringer et al. (2007), and Sun et al. (2009), where the dynamical equilibrium assumption can be fairly applied to derive total mass. Then, using  $M_{\text{tot}} - M_{\text{gas}}$  relation stated in Eq. 1, we can recover the total mass of our sample. In this way, for the non-relaxed clusters, the total mass can be quite accurately determined ( $\sim 10\%$ , Nagai et al. 2007; Zhang et al. 2008). Also, according to numerical simulations (e.g., Nagai et al. 2007), the total ICM mass is measured quite accurately ( $< 6\%$ ) in all clusters, irrespective to the dynamical state.

We also should highlight that the way the total mass was computed from the scaling relation,  $\log M_{\text{tot}} = A + B \times \log M_{\text{gas}}$ , one obtains  $M_{\text{tot}} = 10^A \times M_{\text{gas}}^B$ , and  $f_{\text{gas}} = M_{\text{gas}}/M_{\text{tot}} = 10^{-A/B} \times (M_{\text{tot}})^{(1-B)/B}$ . Thus, being  $f_{\text{gas}} \propto (M_{\text{tot}})^{(1-B)/B}$ , when  $B$  is positive and lower than 1, the gas mass fraction increases with total mass. Since we obtained  $B = 0.827$ , we assume  $f_{\text{gas}} \propto M_{\text{tot}}^{0.2}$ .

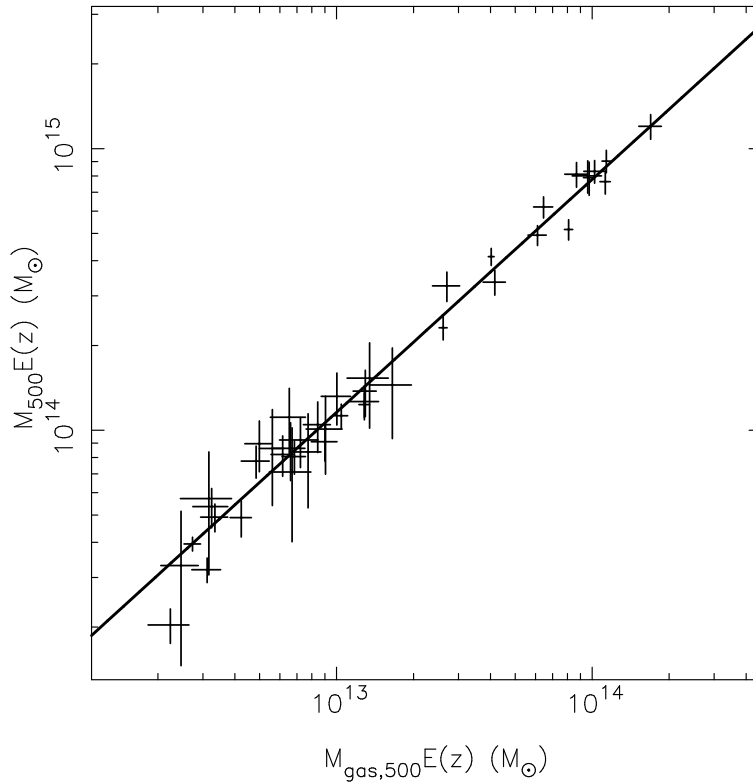


FIG. 1.— Total mass as a function of gas mass for 41 groups and clusters. The continuous line is the power-law fit for the data.

### B. COLOR-MAGNITUDE DIAGRAMS AND THE LUMINOSITY FUNCTION FITS

The elliptical galaxies in individual clusters form a red-sequence (RS) with a well-defined slope and small scatter (Bower et al. 1992b,a). Specifically, the existence of the red-sequence at higher redshifts indicates that cluster elliptical galaxies are a passively evolving population in which the reddening of massive galaxies is the result of a mass-metallicity relation rather than an age effect (Kodama & Arimoto 1997; Kauffmann & Charlot 1998). From the observational point-of-view, studies have shown that for nearby clusters ( $z < 0.05$ ) the slope of the red-sequence is almost constant (Gladders et al. 1998; Romeo et al. 2008). Since we have almost half of the clusters in our sample with redshifts higher than the above mentioned redshift, we did not fix the slope of the RS but left it to vary. We show in Figure B.1 the red-sequence for all clusters in our sample. Even not fixing the slope, we obtained well-defined red-sequence in which the mean slope is  $b = -0.036 \pm 0.010$ .

For all galaxies belonging to the cluster, we build the luminosity function. The luminosity function is the distribution of all morphological types of cluster galaxies over the magnitude. This distribution is generally fit by the Schechter function (Schechter 1976). In Figure B.1, we present the luminosity function fits for all nineteen clusters. In particular, the slope of the faint end of the LF is a direct indicator of the importance of dwarf galaxies, which are expected to be more fragile in the environment of clusters. The great majority of studies of the LF indicate faint-end slopes in the range of  $-0.9$  to  $-1.5$ , but these mostly did not reach very faint magnitudes (see Table 1 in De Propris et al. 2003, and references therein). Recent studies using deep imaging has shown deep estimations of the faint-end slope within the range  $-2.29 < \alpha < -1.07$  (see Table A1 from Boué et al. 2008, and references therein). Our mean values for the slope of the bright population and of the faint-end are  $< \alpha_1 > = -1.28 \pm 0.18$  and  $< \alpha_2 > = -1.72 \pm 0.13$ , respectively. For the characteristic magnitude we obtained  $M_1^* = -22.16 \pm 0.50$  and  $M_2^* = -18.97 \pm 0.85$  for the bright- and for the faint-end, respectively.

### C. IMPACT OF SYSTEMATIC UNCERTAINTIES IN THE PHOTOMETRIC RESULTS

One of the basic observational result of the present study is the stellar masses estimate. To correct determine the stellar mass we followed the description in Sec. 2.2, and here we will discuss the principal steps that account for the systematic uncertainties involved in the total optical luminosity and stellar mass estimates. These systematic uncertainties are summarized in Table 3. First, we can mention that the stellar masses derived from photometric DR7 data can be systematic biased low due to the offset between photometric and spectroscopic magnitudes. This bias can account for  $\sim 10\%$  of uncertainty (Fritz et al. 2011). Then, we can highlight the impact of assuming one Schechter function to describe the overall distribution when one have a steep population faintward. This can affect the determination of  $M^*$  and  $\alpha$  parameters. When not using two functions, the determination of these parameters can systematic bias up the total luminosity determination by  $6 - 15\%$ , what will be directly translated to the  $M^*$  estimates. Also related to the Schechter fit, we can adress the systematics of the covariance between  $M^*$  and  $\alpha$  parameters. If not taken into account, the uncertainties related to these parameters can biased low the total luminosity estimates by about  $5\%$ . The major systematic effect may be introduced by the adopted IMF when assuming a mass-to-light ratio to obtain the stellar mass. For instance, a change from a standard Salpeter (1955) to Kroupa (2001) IMF increases the  $M/L$  by a factor of two. This translates into an increase by the same amount in the stellar mass in our systems. Finally we can adress the ICL contribution. In this work, we did not consider the total light contribution to the stellar mass estimates. Thus, our values can be  $2\%$  systematic biased low (see Sect. 3.1).

TABLE 3  
MAIN SYSTEMATIC UNCERTAINTIES IN STELLAR MASS DETERMINATION

uncertainty	% (approx.)
photometric magnitude	-10
Schechter fit	+ 6-15
covariance between $M^*$ and $\alpha$	-5
IMF	+100
not considering ICL	-2

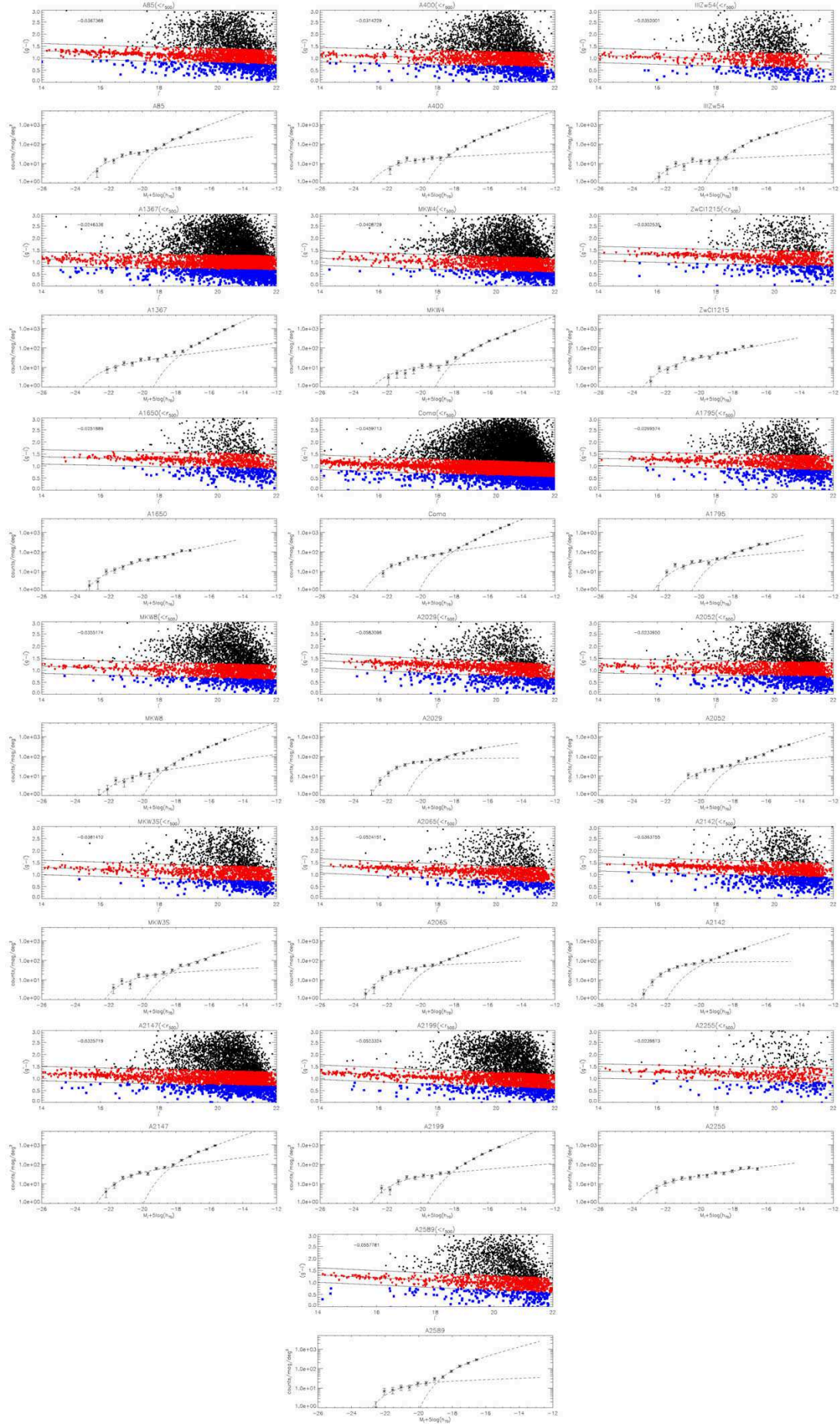


Fig. B.1.— Color-magnitude diagrams and luminosity function fits for our sample.